



PAPER

## Assessing bioink shape fidelity to aid material development in 3D bioprinting

To cite this article: A Ribeiro *et al* 2018 *Biofabrication* **10** 014102

View the [article online](#) for updates and enhancements.

### Related content

- [Proposal to assess printability of bioinks for extrusion-based bioprinting and evaluation of rheological properties governing bioprintability](#)  
Naomi Paxton, Willi Smolan, Thomas Böck et al.
- [Bioink properties before, during and after 3D bioprinting](#)  
Katja Hölzl, Shengmao Lin, Liesbeth Tytgat et al.
- [Yield stress determines bioprintability of hydrogels based on gelatin-methacryloyl and gellan gum for cartilage bioprinting](#)  
Vivian H M Mouser, Ferry P W Melchels, Jetze Visser et al.

# Biofabrication



## PAPER

# Assessing bioink shape fidelity to aid material development in 3D bioprinting

RECEIVED  
2 May 2017

REVISED  
4 September 2017

ACCEPTED FOR PUBLICATION  
4 October 2017

PUBLISHED  
30 November 2017

A Ribeiro<sup>1,6</sup> , M M Blokzijl<sup>1,2,6</sup>, R Levato<sup>1</sup>, C W Visser<sup>3</sup>, M Castillo<sup>1,4</sup>, W E Hennink<sup>2</sup>, T Vermonden<sup>2</sup> and J Malda<sup>1,5</sup> 

<sup>1</sup> Department of Orthopaedics, University Medical Center Utrecht, Utrecht, The Netherlands

<sup>2</sup> Department of Pharmaceutics, Utrecht Institute for Pharmaceutical Sciences (UIPS), Faculty of Science, Utrecht University, Utrecht, The Netherlands

<sup>3</sup> Harvard John A. Paulson School of Engineering and Applied Sciences, Harvard University, Cambridge, MA, United States of America

<sup>4</sup> Orthopaedic Biomechanics, Department of Biomedical Engineering, Eindhoven University of Technology, Eindhoven, The Netherlands

<sup>5</sup> Department of Equine Sciences, Faculty of Veterinary Medicine, Utrecht, The Netherlands

<sup>6</sup> These authors contributed equally to this work.

E-mail: [j.malda@umcutrecht.nl](mailto:j.malda@umcutrecht.nl)

**Keywords:** bioprinting, bioink, hydrogel, yield stress, extrusion, shape fidelity

Supplementary material for this article is available [online](#)

## Abstract

During extrusion-based bioprinting, the deposited bioink filaments are subjected to deformations, such as collapse of overhanging filaments, which compromises the ability to stack several layers of bioink, and fusion between adjacent filaments, which compromises the resolution and maintenance of a desired pore structure. When developing new bioinks, approaches to assess their shape fidelity after printing would be beneficial to evaluate the degree of deformation of the deposited filament and to estimate how similar the final printed construct would be to the design. However, shape fidelity has been prevalently assessed qualitatively through visual inspection after printing, hampering the direct comparison of the printability of different bioinks. In this technical note, we propose a quantitative evaluation for shape fidelity of bioinks based on testing the filament collapse on overhanging structures and the filament fusion of parallel printed strands. Both tests were applied on a hydrogel platform based on poloxamer 407 and poly(ethylene glycol) blends, providing a library of hydrogels with different yield stresses. The presented approach is an easy way to assess bioink shape fidelity, applicable to any filament-based bioprinting system and able to quantitatively evaluate this aspect of printability, based on the degree of deformation of the printed filament. In addition, we built a simple theoretical model that relates filament collapse with bioink yield stress. The results of both shape fidelity tests underline the role of yield stress as one of the parameters influencing the printability of a bioink. The presented quantitative evaluation will allow for reproducible comparisons between different bioink platforms.

## 1. Introduction

Biofabrication is a rapidly growing field that aims to develop sophisticated constructs for tissue regeneration and *in vitro* models through bioprinting or bioassembly of living cells and biomaterials [1, 2]. These approaches hold the potential to achieve functional tissue constructs by replicating the complex architecture and organization of native tissues [3, 4]. As such, precise placement of cells and materials and the resulting construct shape fidelity are fundamental parameters.

Among several biofabrication techniques, extrusion-based bioprinting of cell-laden hydrogels is one of the most widely explored techniques. Using different extrusion methods, i.e. pneumatic or mechanical via piston or screw-driven systems, it is possible to print a wide range of materials to create constructs with high cell densities [5–7].

The printed filaments are the elemental building blocks in extrusion-based 3D bioprinting and their formation is thus a critical step in the bioprinting process. Besides appropriate hardware and software, accurate and controlled filament deposition requires

careful selection of the bioink according to its rheological properties. Ideally, a hydrogel for printing should display shear thinning behavior, that is, its viscosity decreases with increasing shear rate [7]. Equally important is the presence of yield stress and quick recovery kinetics, so the polymer behaves as a non-viscous liquid during extrusion and a shape stable gel is quickly formed after deposition [6].

However, the design of high-performance-bioinks is a challenging task, since there needs to be a compromise between adequate rheological properties to maintain shape fidelity of a printed construct and material biocompatibility that allows the proliferation, differentiation and biosynthetic activity of cells or tissue [6]. Therefore, when experimenting with a new bioink, its printability should be carefully evaluated in order to assess physical deformation of the deposited filament, predict shape fidelity of the printed structure and gain control over precise filament deposition on the printing plane. Despite the need for and importance of evaluation, there is no consensus on approaches to assess or predict shape fidelity, let alone printability.

Although in the field of bioprinting the term printability is not univocally defined, for the purpose of this study we refer to this property as the possibility to extrude a hydrogel, and dispense it in a pattern with a satisfactory degree of shape fidelity, the latter indicating how the printed structure is matching the original CAD design. As such, shape fidelity is a key aspect of printability, and its standardized and quantitative description would significantly aid the development of new bioinks.

To date, shape fidelity has predominantly been determined from visual qualitative evaluation of either extruded filaments [8] or printed structures from macro- and microscopic images [9–17]. Although these approaches for *post hoc* evaluation provide a first impression on the resolution of the printed outcome, they are highly subjective and exclusive to the gels being studied. Therefore, they do not allow for proper comparison between different bioinks or even between studies involving the same bioink. This lack of comparability underscores the need to establish a reproducible universal testing methodology, which could be used to assess the ability to retain the designed shape.

Some progress towards a reproducible and quantitative testing methodology has recently been made. For instance, Ouyang *et al* proposed a method based on circularity of pores in the lattice of constructs printed with a  $0^{\circ}$ – $90^{\circ}$  lay-down pattern. In this case, low pore circularity was used as an indicator of higher printability, as the produced pores are closer to the shape of the design [18]. Such outcome, however, only deals with one component of shape fidelity, which is the resolution in the  $x$ – $y$  plane and does not take deformation of the printed filament due to sagging of

overhanging structures as well as the role of rheological properties in account.

Bioinks are generally mechanically soft and viscoelastic in nature. As a consequence, during the bioprinting process a deposited bioink filament is subjected to deformations. More specifically, sagging or collapse of the suspended filaments can occur due to the viscoelastic behavior of the soft material [19]. In addition, pore closure can occur due to fusion between adjacent filaments after printing [18, 20]. The two main forces underlying these phenomena are gravity, leading to overall loss of structure due to compression or sagging, and surface tension, causing filaments to adopt shapes that minimize surface area [21].

Therefore, in this technical note an approach to evaluate bioink shape fidelity is presented through two quantitative tests based on filament deformation after printing: (i) filament collapse, assessing the deflection and collapse of a suspended filament, and (ii) filament fusion, assessing resolution of the printed filaments in the  $x$ – $y$  plane. To demonstrate the functionality of the proposed tests, gels based on poloxamer 407 were selected as reproducible model bioink, as these gels exhibit excellent properties for 3D printing [22–27]. Specifically, a small hydrogel library of gels having different yield stresses was generated by blending poloxamer with poly(ethylene glycol) (PEG).

Moreover, we aimed to highlight the relationship between the results of the proposed tests and the hydrogel rheological properties and shape fidelity. For instance, it was recently demonstrated that high yield stress, in combination with a fast drop in viscosity by shear thinning during extrusion, leads to optimal printability in gelMA/gellan gum bioinks [28]. Therefore, we propose a simple theoretical model in order to predict filament collapse directly from yield stress.

## 2. Materials and methods

### 2.1. Hydrogels preparation

Poloxamer gels were prepared by adding poloxamer 407 (poloxamer, Sigma Aldrich) and (PEG,  $M_n = 10$  kDa, Sigma Aldrich) to phosphate buffered saline solutions (pH 7.4). These were left to dissolve under mild agitation at a temperature of  $4^{\circ}\text{C}$  for 48 h. To enable visualization and imaging of the hydrogels, two different colored gels were prepared for each formulation by adding either 0.1 wt% tartrazine (E102, Sigma Aldrich) yellow food dye or 0.1 wt% new coccine (E124, Sigma Aldrich) red dye. These hydrogels were prepared in concentrations ranging between 20% and 30%. Total polymer concentration was kept at 30% by substituting the decreasing amount of poloxamer with PEG and yield stress was recorded for each solution. The yield stress could not be determined for solutions with PEG concentrations above 4%, indicating that these solutions did not form a gel at room

temperature. For this reason, the 20% poloxamer sample was not supplemented with PEG, and the solutions used in the presented shape fidelity tests are, according to the concentration of poloxamer/PEG: 30%/29/1%, 28/2%, 27/3%, 26/4% and 20%.

## 2.2. Rheological evaluation

Yield stress measurements were performed on a DHR2 rheometer (TA Instruments, The Netherlands), equipped with a stainless-steel cone/plate system (40 mm diameter, 2° cone angle and truncation gap of 54  $\mu\text{m}$ ). Samples were equilibrated at a temperature of 21 °C for 10 s, followed by exposure to shear flow peak hold at a rate of 300  $\text{s}^{-1}$  for 10 s to simulate shear in a 3D printer nozzle. Viscosity was recorded during flow peak hold and measured as the average viscosity of 10 points. Subsequently, samples were subjected to an oscillatory stress sweep ranging from 10 to 1000 Pa, at a frequency of 1 Hz. Storage ( $G'$ ) and loss modulus ( $G''$ ) were recorded during oscillatory stress sweep, and yield stress was defined as the crossover point between  $G'$  and  $G''$  and determined by interpolation using TRIOS software (TA Instruments). Each measurement was performed three times.

## 2.3. Filament collapse test

The filament collapse test is based on work by Therriault *et al* where the mid-span deflection of a suspended filament of organic inks was assessed [19]. A platform with pillars ( $l \times w \times h = 2.0 \times 2.0 \times 4.0$  mm) placed at known gap distances (1.0, 2.0, 4.0, 8.0 and 16.0 mm) between each other was designed (CAD file in supplementary info is available online at [stacks.iop.org/BF/10/014102/mmedia](https://stacks.iop.org/BF/10/014102/mmedia)), and constructed on a Perfactory Mini digital light projection 3D printer (Envisiontec, Germany) using a proprietary PIC100 resin. Over these gaps a single gel filament was deposited (g-code in supplementary info) using a 3D Discovery bioprinter (RegenHU, Switzerland), while the process was recorded using a USB microscope (Bresser, Germany) at a magnification of 20 $\times$ , a frame rate of 30 fps and a resolution of 640  $\times$  480 pixels. Gels were loaded at 4 °C into 3 ml syringe barrels (Nordson EFD, UK) and extruded using a 23 Gauge straight metal nozzle (Nordson EFD) having an inner diameter of 0.33 mm. To ensure an average filament diameter of around 0.3 mm throughout all samples, the deposition speed was fixed at 6  $\text{mm s}^{-1}$  and air pressure was adjusted correspondingly for each different concentration (20%–60 kPa; 26/4%–70 kPa; 27/3%–90 kPa; 28/2%–120 kPa; 29/1%–130 kPa; 30%–160 kPa). The nozzle-tip was placed at 0.3 mm above the top surface of the pillars and the print path extended until 10 mm after the last pillar.

The deflection of the filament was quantified by measuring the angle of deflection  $\theta$  at the edge of the suspended filament from video stills using FIJI

software (version 1.51k, NIH, USA) at time  $t = 0$  s and  $t = 20$  s after deposition of the whole filament, as no apparent deformation occurred after that time point. Angle  $\theta$  was plotted against half the spanning distance  $L$  for stills obtained at  $t = 20$  s. The plotted points represent the mean with standard deviation for 3 repetitions of the test for each formulation.

## 2.4. Filament fusion test

The filament fusion test consists of printing three layers of a meandering pattern composed of parallel strands at increasing spacing. To facilitate visualization, the first and second layer were printed with yellow-stained hydrogels, while the third with the red-stained ones. Measurements were performed on this third layer to avoid unwanted gel spreading caused by the glass surface and its associated surface tension. The pattern starts at a filament distance of 0.25 mm, increases 0.05 mm for each subsequent line, and finishes at the distance of 0.55 mm (g-code in supplementary info). To ensure an average filament diameter of around 0.30 mm throughout all samples, the deposition speed was fixed at 13  $\text{mm s}^{-1}$  and air pressure was adjusted for each concentration (20%–80 kPa; 26/4%–90 kPa; 27/3%–120 kPa; 28/2%–150 kPa; 29/1%–170 kPa; 30%–200 kPa). This change in the deposition speed compare to the suspended filament test was applied to account for the difference in the printing substrate between the two tests. Other printing settings were identical to those in the suspended filament test. Top-down pictures were obtained using a stereo microscope (Olympus SZ61, magnification 4.2 $\times$ , resolution 2040  $\times$  1536 pixels) directly after printing, as no apparent deformation was observed at this time point. The length of the fused filament at the top and bottom edges of the meandering pattern was measured using FIJI software, and plotted for each filament distance. The plotted values represent the mean of measurements over 3 repetitions of the test for each formulation.

## 2.5. Theoretical model for filament collapse

In order to correlate yield stress with the outcome of filament collapse, a simple predictive model was created. After 20 s of printing, it is assumed that deformation is negligible and the forces acting on the filament reached an equilibrium. Assuming that the cross-sectional area of the filament maintains constant, the equation of equilibrium can be written as,

$$F_g + F_\sigma = 0, \quad (1)$$

where  $F_g$  represents the gravitational force and  $F_\sigma$  the force resulting from the material resistance to yield. Looking at the equilibrium in the vertical direction, the equation (1) can be rewritten as,

$$F_g - F_\sigma \sin \theta = 0, \quad (2)$$

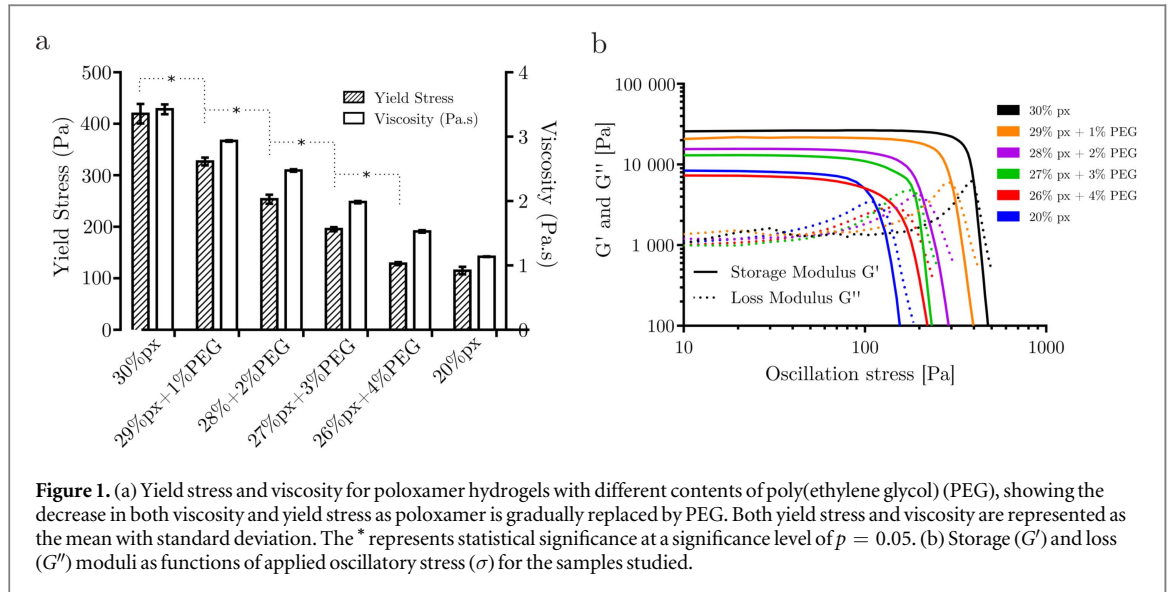


**Figure 1.** (a) Yield stress and viscosity for poloxamer hydrogels with different contents of poly(ethylene glycol) (PEG), showing the decrease in both viscosity and yield stress as poloxamer is gradually replaced by PEG. Both yield stress and viscosity are represented as the mean with standard deviation. The \* represents statistical significance at a significance level of  $p = 0.05$ . (b) Storage ( $G'$ ) and loss ( $G''$ ) moduli as functions of applied oscillatory stress ( $\sigma$ ) for the samples studied.

where  $\theta$  is the angle of deflection of the filament with the horizontal direction. Therefore, considering the forces are being exerted on an infinitesimal volume element  $\delta V$ , equation (2) takes now the form,

$$\frac{F_g}{\delta V} - \frac{F_\sigma}{\delta V} \sin \theta = 0. \quad (3)$$

The angle of deflection  $\theta$  can then be related with the stresses acting on the volume  $\delta V$  by,

$$\frac{mg}{\delta V} - \frac{F_\sigma}{\delta A \cdot L} \sin \theta, \quad (4)$$

where  $m$  is the filament mass,  $L$  the distance from the edge of the pillar to the midpoint of the suspended filament, and  $\delta A$  an infinitesimal cross-sectional area of the filament. Equation (4) can be rewritten as,

$$\theta = \sin^{-1} \left( \frac{\rho g L}{\sigma_{\text{yield}}} \right), \quad (5)$$

where  $\rho$  is the density of the material, which is approximately  $1020 \text{ kg m}^{-3}$  for the poloxamer 407 samples prepared,  $g$  is the gravitational acceleration, which is approximately  $9.8 \text{ m s}^{-2}$ , and  $\sigma_{\text{yield}}$  denotes the yield stress of the hydrogel.

## 2.6. Statistics

Data are presented as mean  $\pm$  standard deviation. To assess statistical significance of differences in yield stress, viscosity, filament fusion and collapse tests the distribution of values for both quantities was assumed to be normal, and a two-way ANOVA was performed at a significance level of  $p = 0.05$ . This was followed by *post hoc* Tukey's test to find statistical significant differences between the values of yield stress and viscosity for the different poloxamer/PEG concentrations.

## 3. Results

### 3.1. Rheological properties

The rheological analysis showed that a decrease in the concentration of poloxamer 407 with subsequent increase in the concentration of PEG led to a decrease in both viscosity and yield stress (figure 1(a))—between 30% and 20%, there was approximately a 3-fold decrease in viscosity and a 4-fold decrease in yield stress. Analogously, the elastic modulus  $G'$  plateau also followed the same trend as viscosity and yield stress, although the  $G'$  plateau in the 20% sample was higher than the one obtained for the 26/4% sample (figure 1(b)).

### 3.2. Qualitative assessment of shape fidelity

When a simple qualitative visual inspection was performed, the differences between the design (figures 2(a)–(c)) and the printed constructs became clear, with special attention to differences in lateral porosity caused by collapse of overhanging filaments and to differences in the shape of the pores in the  $x$ – $y$  plane. The difference in shape fidelity was apparent when porous constructs were produced with a hydrogel with high yield stress, i.e. the 30% poloxamer (figures 2(d)–(f)), and a hydrogel with a lower yield stress, i.e. the 20% poloxamer (figures 2(g)–(i)).

### 3.3. Quantitative assessment of shape fidelity

#### 3.3.1. Filament collapse test

The filament collapse test (figure 3(a)) revealed that filament sagging increased as the gap length increased, as observed by the increase in the deflection angle  $\theta$ . Further, an increase in the concentration of poloxamer and, consequently, an increase in yield stress, led to a decrease in sagging (figures 3(b) and (c), and supplementary videos 1 and 2).

For each condition, a linear regression was performed. The resulting linear regression plots of the

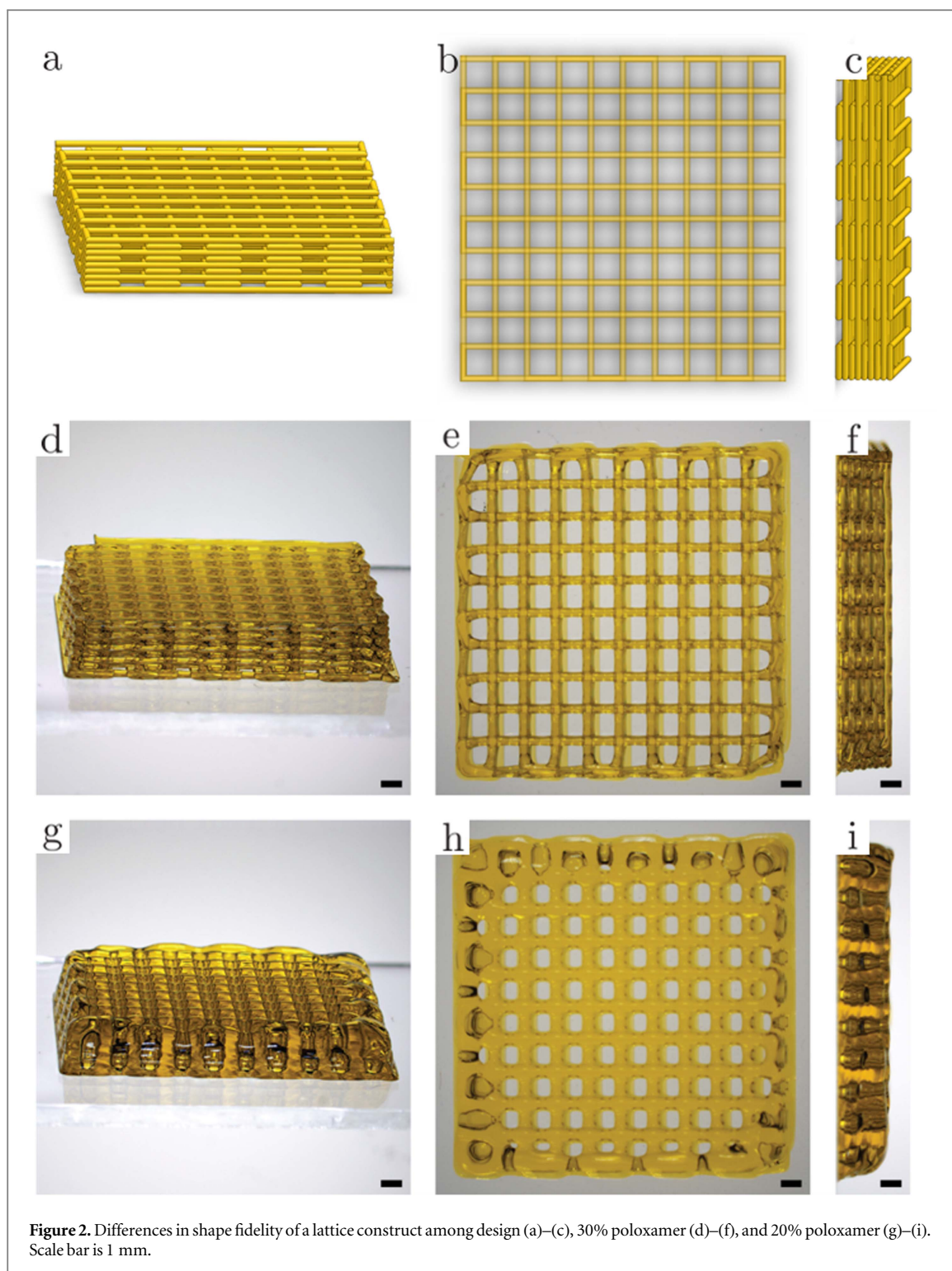


**Figure 2.** Differences in shape fidelity of a lattice construct among design (a)–(c), 30% poloxamer (d)–(f), and 20% poloxamer (g)–(i). Scale bar is 1 mm.

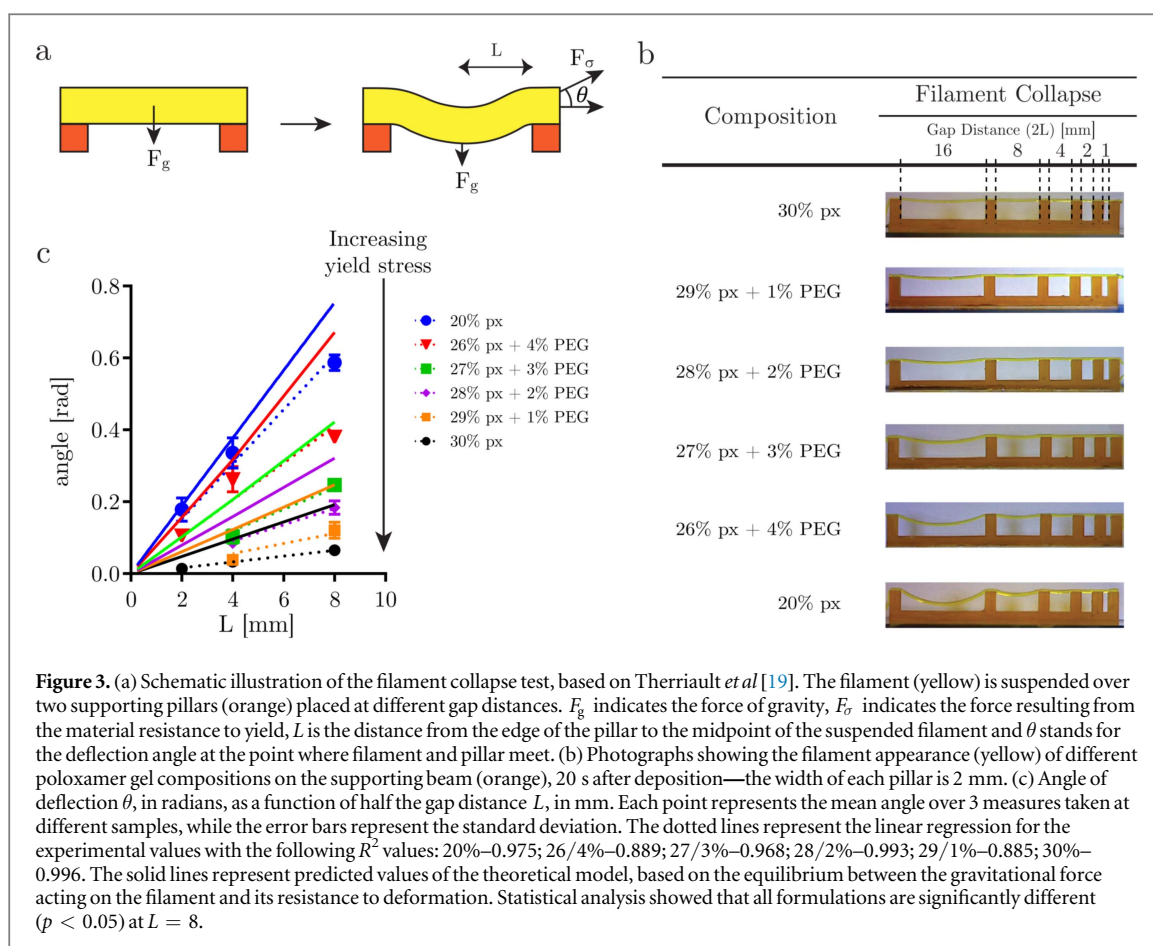
different concentrations demonstrated that with increasing concentration, i.e. yield stress, the slope of each line decreased (figure 3(c)).

To further relate yield stress with the collapse of filaments, the deflection angle for each gap distance was calculated using the theoretical model represented in equation (5) and the resulting theoretical values were compared with the ones obtained experimentally (figure 3(c)). Although the model overestimated the angle of deflection, the slope of the regression lines for

the theoretical values followed the same trend as the experimental ones.

### 3.3.2. Filament fusion test

To assess the effect of filament fusion and pore closure for each gel concentration, the fused segment length  $f_s$  was measured at each filament distance  $f_d$  (figures 4 and 5). In order to discard the effect of filament thickness ( $f_t$ ) variation between different concentrations of poloxamer,



fs was normalized by dividing it by the average ft in each sample.

This test was initially performed with one layer of hydrogel deposited directly on the glass substrate (figure 4). In order to circumvent the influence of the glass surface on the wetting behavior of the gel, measurements were subsequently done on a third layer deposited on top of the gel (figure 5).

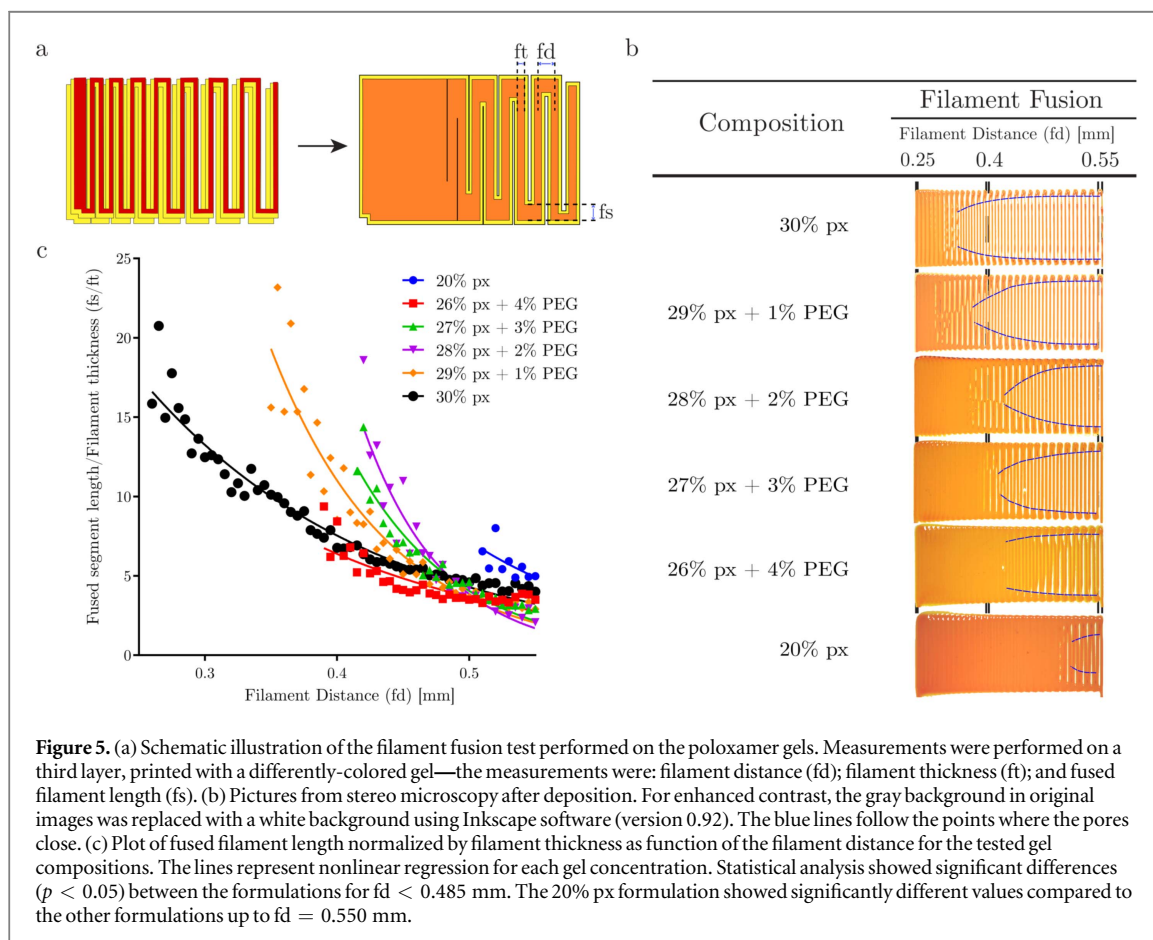
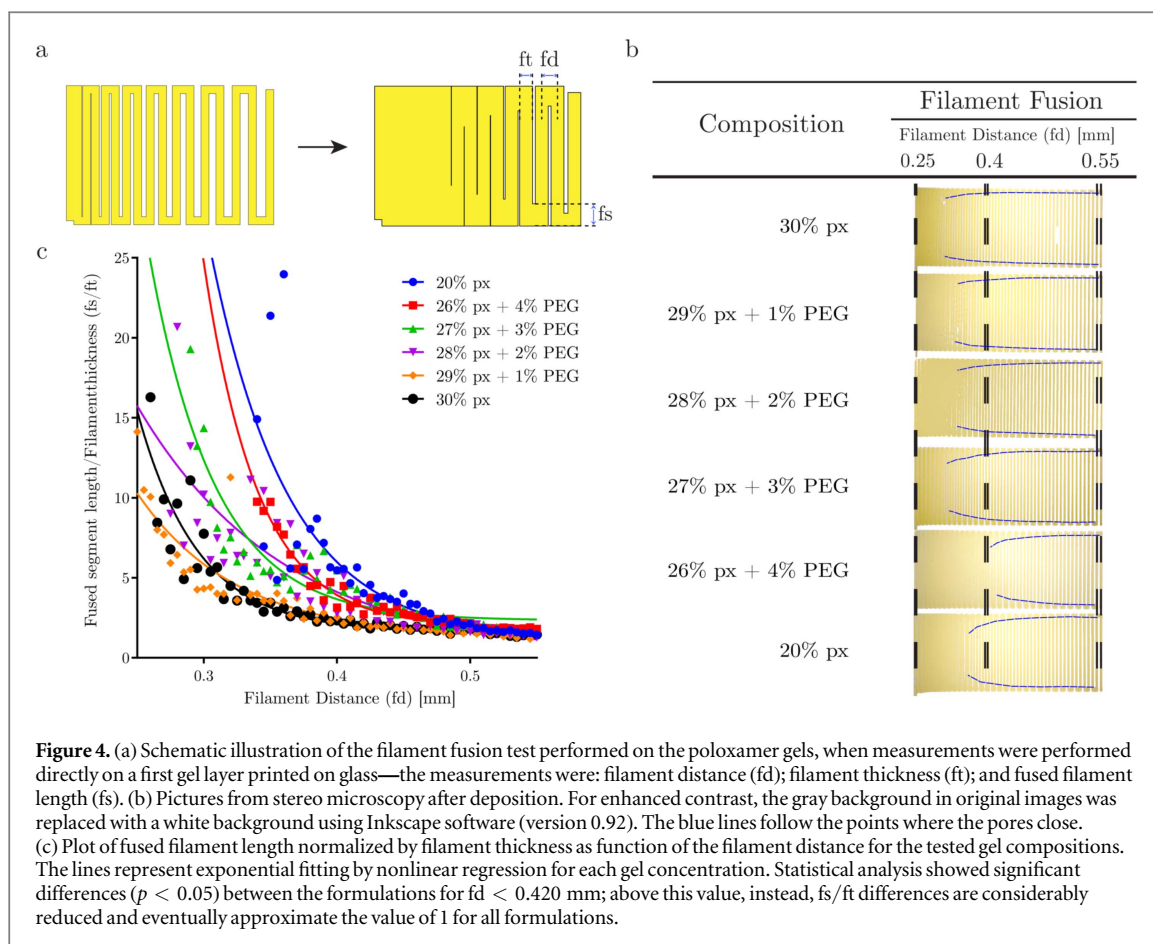
As fd decreased, an increase in fs was observed for all samples. Fitting of the data suggested a nonlinear inverse relation between the fused segment length fs and the filament distance fd. Among the different poloxamer/PEG concentrations, fs tended to increase at higher values of fd for lower concentrations of poloxamer. This increase in fs could be observed macroscopically when comparing the printed meandering patterns between the different poloxamer/PEG concentrations, as the points where the pores closed, highlighted with the blue lines in figures 4(b) and 5(b), also revealed a similar trend to the one plotted on figures 4(c) and 5(c).

#### 4. Discussion

In this study, a versatile strategy for testing and characterizing the shape fidelity of bioinks for extrusion-based biofabrication was introduced, consisting of a toolbox of experiments that can be easily adopted for multiple hydrogel formulations.

The assessment of printability during the development of new bioinks has mainly been performed by qualitative visual inspection of printed constructs. Such observation is a quick way to establish the relative shape fidelity and distinguish results for different concentrations of a gel formulation. However, this qualitative inspection does not allow for reproducible comparisons between different hydrogels. Although visual differences are also clear between the 20% and 30% poloxamer hydrogels in this study, they were macroscopically less obvious for the intermediate poloxamer/PEG concentrations. Nevertheless, the results of the tests presented in this technical note reproducibly showed clear differences in shape fidelity between the different concentrations of the hydrogel system.

For the filament collapse test, the angle of deflection decreased with increasing poloxamer concentration. This trend can be explained by the increase in hydrogel yield stress along with storage modulus, which made the hydrogel filaments more resistant to deformation from collapse. The deformation of the suspended filaments was initiated by the weight of the material. Nonetheless, surface tension and viscoelasticity of the gel counteract the deformation caused by gravity [21]. This may have led to the overestimation of the angle of deflection by our simplified model, as it only takes into account the force of gravity and yield stress of the hydrogel.



The angle of deflection in the filament collapse test was measured 20 s after printing for every hydrogel sample. Although no significant filament collapse can be observed after this time point, it should be noted that deformation still continues at a slower rate, as observed in creep analysis of the hydrogels for 24 h (data not shown). Nonetheless, such slow deformation can be disregarded since printing time periods are generally in the order of minutes, after which gels are either crosslinked or, when used as sacrificial material, removed [6].

For the filament fusion test, there was a clear relationship between the evolution of pore closure and the concentration of poloxamer. As poloxamer was replaced by PEG, the minimum pore size increased, that is, the resolution obtained with the hydrogel decreased. The printed meandering pattern in this test can provide a more objective and quantifiable assessment of the relative filament resolution than the macroscopic evaluation of 3D constructs, as it is possible to assess the minimum pore size achievable for each hydrogel tested.

Pore closure occurs especially for soft materials and sharp corners, i.e. small pores. In these cases, the capillary forces exceed the yield stress of the material, resulting in deformation of these corners which progresses until the capillary forces and the yield stress balance [29]. Initial experiments were performed on glass, but here the pinning of the gel-glass contact line strongly affected the measurements. As more layers are printed, the resulting pattern will only depend on the bioink material itself, which eliminates the variability that the printing platform may introduce. This test is reproducible and generic, but a predictive model based on a balance between yield stress and surface tension could not fully capture the observed deformations. This suggests that not only capillary forces and yield stress, but also gravity and time-dependent effects play an important role in the deformation behavior of bioinks [19, 21]. This is particularly important when considering that bioinks are obtained using hydrogels with very heterogeneous rheological profiles, and that due to this complexity yield stress is an important indicator, but may not be a sufficient predictor for all the families of hydrogel bioinks. Therefore, future work should focus on effective yet accessible models to predict pore closure as a function of the material properties.

The proposed tests provide useful quantitative information on the physical deformation of the bioink, which cannot be obtained from simple visual inspection of extruded filaments [8] or of printed structures [9, 12]. Even though the tests do not isolate a single force that drives the deformation, their outcomes are independent of printing parameters and can be used to compare different bioinks. This greatly differs from other approaches described in the literature [30, 31] where the influence of printing parameters, such as pressure, material feed rate, nozzle size or

nozzle-to-substrate distance, on printability is explored. Although these provide a step-by-step optimization of printing parameters for a certain bioink, they are time consuming, and only specific to the printing systems used. The proposed tests further build upon the quantitative approach introduced by Ouyang *et al* that assessed the reproducibility of a designed pore lattice [18]. The presented tests in this technical note could be used to evaluate the potential shape fidelity of a bioink based on the collapse and fusion of filaments, aiding the engineering of bio-printed constructs for tissue engineering.

## 5. Conclusion

The shape fidelity tests in this work present a readily accessible and reproducible methodology to quickly test new material formulations and compare them with established ones. This may substantially accelerate the development of new bioinks by directly assessing their performance. Both tests quantitatively evaluate shape fidelity according to the physical deformation of printed bioink filaments, which up till now is mostly only qualitatively assessed and interpreted subjectively by performing visual inspection. For the development of new bioink platforms, this testing methodology accompanied with extensive rheological characterization will provide further insights into the influence of rheological properties on shape fidelity. However, the proposed approach focuses on the structural properties of bioinks. Although assessing aspects of printability during the development of a bioink is crucial to fabricate constructs with more complex architectural organization, the biological performance of the materials should also always be assessed, for instance through post-printing cell viability and functionality studies.

Taken together, the results underscore the important role of yield stress on hydrogel shape fidelity. While several material properties, namely viscosity and storage modulus, are determinant to print constructs with high shape fidelity, yield stress could be used as a relevant parameter to predict filament deformation and estimate shape fidelity. Although the predictive model overestimates filament collapse when compared to the experimental data, the same relation of shape fidelity between the different concentrations tested is maintained, paving the way for future work on theoretical models that may be used to quantify printability parameters directly from hydrogel rheological properties.

## Acknowledgments

The research leading to this work has received funding from the European Community's Seventh Framework Programme (FP7/2007-2013) under grant agreement no. 309962 (HydroZONES), the European Research

Council under grant agreement no. 647426 (3D-JOINT).

#### Author contributions

MMB, RL, CWV, TV, JM conceived and initiated the project. AR, MMB, RL, MC, WEH, TV, JM designed the experiments. AR and MMB performed the experiments. AR, MMB, RL, MC, WEH, TV, JM analyzed the data. AR and MMB wrote the paper with inputs from all authors.

#### ORCID iDs

A Ribeiro  <https://orcid.org/0000-0001-5838-6725>

J Malda  <https://orcid.org/0000-0002-9241-7676>

#### References

- [1] Groll J et al 2016 Biofabrication: reappraising the definition of an evolving field *Biofabrication* **8** 13001
- [2] Mironov V, Trusk T, Kasyanov V, Little S, Swaja R and Markwald R 2009 Biofabrication: a 21st century manufacturing paradigm *Biofabrication* **1** 22001–16
- [3] Mouser V H M, Levato R, Bonassar L J, DLima D D, Grande D A, Klein T J, Saris D B F, Zenobi-Wong M, Gawlitta D and Malda J 2016 Three-dimensional bioprinting and its potential in the field of articular cartilage regeneration *Cartilage* **8** 327
- [4] Ozbolat I T and Hospodiuk M 2016 Current advances and future perspectives in extrusion-based bioprinting *Biomaterials* **76** 321–43
- [5] Derby B 2012 Printing and prototyping of tissues and scaffolds *Science* **338** 921–6
- [6] Malda J, Visser J, Melchels F P, Jungst T, Hennink W E, Dhert W J A, Groll J and Huttmacher D W 2013 25th anniversary article: engineering hydrogels for biofabrication *Adv. Mater.* **25** 5011–28
- [7] Jungst T, Smolan W, Schacht K, Scheibel T and Groll J 2016 Strategies and molecular design criteria for 3D printable hydrogels *Chem. Rev.* **116** 1496–539
- [8] Schuurman W, Levett P A, Pot M W, van Weeren P R, Dhert W J A, Huttmacher D W, Melchels F P W, Klein T J and Malda J 2013 Gelatin-methacrylamide hydrogels as potential biomaterials for fabrication of tissue-engineered cartilage constructs *Macromol. Biosci.* **13** 551–61
- [9] Stichler S, Jungst T, Schamel M, Zilkowski I, Kuhlmann M, Böck T, Blunk T, Teßmar J and Groll J 2017 Thiol-ene clickable poly(glycidol) hydrogels for biofabrication *Ann. Biomed. Eng.* **45** 273–85
- [10] Skardal A et al 2015 A hydrogel bioink toolkit for mimicking native tissue biochemical and mechanical properties in bioprinted tissue constructs *Acta Biomater.* **25** 24–34
- [11] Rees A, Powell L C, Chinga-Carrasco G, Gethin D T, Syverud K, Hill K E and Thomas D W 2015 3D bioprinting of carboxymethylated-periodate oxidized nanocellulose constructs for wound dressing applications *BioMed Res. Int.* **2015** 1–7
- [12] Lee H J, Kim Y B, Ahn S H, Lee J-S, Jang C H, Yoon H, Chun W and Kim G H 2015 A new approach for fabricating collagen/ECM-based bioinks using preosteoblasts and human adipose stem cells *Adv. Healthcare Mater.* **4** 1359–68
- [13] Zhao Y, Li Y, Mao S, Sun W and Yao R 2015 The influence of printing parameters on cell survival rate and printability in microextrusion-based 3D cell printing technology *Biofabrication* **7** 45002
- [14] Kim Y B, Lee H, Yang G-H, Choi C H, Lee D, Hwang H, Jung W-K, Yoon H and Kim G H 2016 Mechanically reinforced cell-laden scaffolds formed using alginate-based bioink printed onto the surface of a PCL/alginate mesh structure for regeneration of hard tissue *J. Colloid Interface Sci.* **461** 359–68
- [15] Colosi C, Shin S R, Manoharan V, Massa S, Costantini M, Barbetta A, Dokmeci M R, Dentini M and Khademhosseini A 2016 Microfluidic bioprinting of heterogeneous 3D tissue constructs using low-viscosity bioink *Adv. Mater.* **28** 677–684a
- [16] Müller M, Ozturk E, Arlov O, Gatenholm P and Zenobi-Wong M 2016 Alginate sulfate-nanocellulose bioinks for cartilage bioprinting applications *Ann. Biomed. Eng.* **45** 210
- [17] Mouser V H M, Abbadessa A, Levato R, Hennink W E, Vermonden T, Gawlitta D and Malda J 2017 Development of a thermosensitive HAMA-containing bio-ink for the fabrication of composite cartilage repair constructs *Biofabrication* **9** 015026
- [18] Ouyang L, Yao R, Zhao Y and Sun W 2016 Effect of bioink properties on printability and cell viability for 3D bioplotting of embryonic stem cells *Biofabrication* **8** 35020
- [19] Therriault D, White S R and Lewis J A 2007 Rheological behavior of fugitive organic inks for direct-write assembly *Appl. Rheol.* **17** 10112
- [20] Chung J H Y, Naficy S, Yue Z, Kapsa R, Quigley A, Moulton S E and Wallace G G 2013 Bio-ink properties and printability for extrusion printing living cells *Biomater. Sci.* **1** 763
- [21] Xu X, Jagota A, Peng S, Luo D, Wu M and Hui C-Y 2013 Gravity and surface tension effects on the shape change of soft materials *Langmuir* **29** 8665–74
- [22] Fedorovich N E, Swennen I, Girones J, Moroni L, Van Blitterswijk C A, Schacht E, Alblas J and Dhert W J A 2009 Evaluation of photocrosslinked lutrol hydrogel for tissue printing applications *Biomacromolecules* **10** 1689–96
- [23] Müller M, Becher J, Schnabelrauch M and Zenobi-Wong M 2015 Nanostructured pluronic hydrogels as bioinks for 3D bioprinting *Biofabrication* **7** 35006
- [24] Kolesky D B, Truby R L, Gladman A S, Busbee T A, Homan K A and Lewis J A 2014 3D bioprinting of vascularized, heterogeneous cell-laden tissue constructs *Adv. Mater.* **26** 3124–30
- [25] Kolesky D B, Homan K A, Skylar-Scott M A and Lewis J A 2016 Three-dimensional bioprinting of thick vascularized tissues *Proc. Natl Acad. Sci. USA* **113** 3179–84
- [26] Melchels F P W, Blokzijl M M, Levato R, Peiffer Q C, de Ruijter M, Hennink W E, Vermonden T and Malda J 2016 Hydrogel-based reinforcement of 3D bioprinted constructs *Biofabrication* **8** 35004
- [27] Levato R, Webb W R, Otto I A, Mensinga A, Zhang Y, van Rijen M, van Weeren R, Khan I M and Malda J 2017 The bio in the ink: cartilage regeneration with bioprintable hydrogels and articular cartilage-derived progenitor cells *Acta Biomater.* **61** 41
- [28] Mouser V H M, Melchels F P W, Visser J, Dhert W J A, Gawlitta D and Malda J 2016 Yield stress determines bioprintability of hydrogels based on gelatin-methacryloyl and gellan gum for cartilage bioprinting *Biofabrication* **8** 35003
- [29] Kokkinis D, Schaffner M, Studart A R, Vermant J and Whitesides G M 2015 Multimaterial magnetically assisted 3D printing of composite materials *Nat. Commun.* **6** 8643
- [30] Kang K H, Hockaday L A and Butcher J T 2013 Quantitative optimization of solid freeform deposition of aqueous hydrogels *Biofabrication* **5** 35001
- [31] He Y, Yang F, Zhao H, Gao Q, Xia B and Fu J 2016 Research on the printability of hydrogels in 3D bioprinting *Sci. Rep.* **6** 29977